Inorg. Chem. **2005**, *44*, 2263–2271

New d^0 Transition Metal Iodates: Synthesis, Structure, and Characterization of $BaTi(IO_3)_6$, $LaTiO(IO_3)_5$, $Ba_2VO_2(IO_3)_4 \cdot (IO_3)$, $K_2MoO_2(IO_3)_4$, and $BaMoO_2(IO_3)_4 \cdot H_2O$

Kang Min Ok and P. Shiv Halasyamani*

Department of Chemistry and Center for Materials Chemistry, 136 Fleming Building, University of Houston, Houston, Texas 77204-5003

Received November 8, 2004

Five new d^0 transition metal iodates, $BaTi(IO_3)_6$, $LaTiO(IO_3)_5$, $Ba_2VO_2(IO_3)_4 \cdot (IO_3)$, $K_2MoO_2(IO_3)_4$, and $BaMoO_2(IO_3)_4 \cdot H_2O$, have been synthesized by hydrothermal methods using $Ba(OH)_2 \cdot 8H_2O$, La_2O_3, K_2CO_3, TiO_2, V_2O_5, MoO_3, and HIO_3 as reagents. The structures of these compounds were determined by single-crystal X-ray diffraction. All of the reported materials have zero-dimensional or pseudo-one-dimensional crystal structures composed of MO_6 ($M = Ti^{4+}$, V^{5+}, or Mo^{6+}) octahedra connected to IO_3 polyhedra. Infrared and Raman spectroscopy, thermogravimetric analysis, and UV–vis diffuse reflectance spectroscopy are also presented. Crystal data: $BaTi(IO_3)_6$, trigonal, space group $R\bar{3}$ (No. 148), with $a = b = 11.4711(10)$ Å, $c = 11.1465(17)$ Å, $V = 1270.2(2)$ Å^3, and $Z = 3$; $LaTiO(IO_3)_5$, monoclinic, space group $P2_1/n$ (No. 14), with $a = 7.4798(10)$ Å, $b = 18.065(2)$ Å, $c = 10.4843(14)$ Å, $\beta = 91.742(2)°$, $V = 1416.0(3)$ Å^3, and $Z = 4$; $Ba_2VO_2(IO_3)_4 \cdot (IO_3)$, monoclinic, space group $P2_1/c$ (No. 14), with $a = 7.5012(9)$ Å, $b = 33.032(4)$ Å, $c = 7.2150(9)$ Å, $\beta = 116.612(2)°$, $V = 1598.3(3)$ Å^3, and $Z = 4$; $K_2MoO_2(IO_3)_4$, monoclinic, space group $C2/c$ (No. 15), with $a = 12.959(2)$ Å, $b = 6.0793(9)$ Å, $c = 17.748(3)$ Å, $\beta = 102.410(4)°$, $V = 1365.5(4)$ Å^3, and $Z = 4$; $BaMoO_2(IO_3)_4 \cdot H_2O$, monoclinic, space group $P2_1/n$ (No. 14), with $a = 13.3368(17)$ Å, $b = 5.6846(7)$ Å, $c = 18.405(2)$ Å, $\beta = 103.636(2)°$, $V = 1356.0(3)$ Å^3, and $Z = 4$.

Introduction

In oxide materials, cationic distortions are the driving force for a host of technologically important physical properties such as ferroelectricity, piezoelectricity, and second-harmonic generation. Two families of cations are commonly observed in distorted oxide environments, octahedrally coordinated d^0 transition metals (Ti^{4+}, Nb^{5+}, W^{6+}, etc.) and lone pair cations (Se^{4+}, Te^{4+}, I^{5+}, etc.). With both families, second-order Jahn−Teller (SOJT) type distortions are thought to be the cause for the cationic displacement.[1−7] For octahedrally coordinated d^0 transition metals, the cationic distortion can occur along an edge (local C_2 direction), face (local C_3 direction), or corner (local C_4 direction) of the octahedron,[8] whereas with the lone pair cation a nonbonded electron pair is observed on the cation that "pushes" away the oxide ligands.[9−17] As previously discussed,[7,18] these cationic displacements can be described as primary distortions. Secondary distortions also occur and are defined as the interaction between the d^0 transition metal octahedron and the lone pair cation polyhedron. We recently reviewed all of the oxide materials that contain octahedrally coordinated d^0 transition metals and lone pair cations and made a number of

* Author to whom correspondence should be addressed. E-mail: psh@uh.edu.

(1) Opik, U.; Pryce, M. H. L. *Proc. R. Soc. London* **1957**, *A238*, 425.
(2) Bader, R. F. W. *Mol. Phys.* **1960**, *3*, 137.
(3) Bader, R. F. W. *Can. J. Chem.* **1962**, *40*, 1164.
(4) Pearson, R. G. *J. Am. Chem. Soc.* **1969**, *91*, 4947.
(5) Pearson, R. G. *J. Mol. Struct. (THEOCHEM)* **1983**, *103*, 25.
(6) Wheeler, R. A.; Whangbo, M.-H.; Hughbanks, T.; Hoffmann, R.; Burdett, J. K.; Albright, T. A. *J. Am. Chem. Soc.* **1986**, *108*, 2222.
(7) Kunz, M.; Brown, I. D. *J. Solid State Chem.* **1995**, *115*, 395.
(8) Goodenough, J. B. *Annu. Rev. Mater. Sci.* **1998**, *28*, 1.
(9) Sidgwick, N. V.; Powell, H. M. *Proc. R. Soc. London* **1940**, *A176*, 153.
(10) Gillespie, R. J.; Nyholm, R. S. *Q. Rev., Chem. Soc.* **1957**, *11*, 339.
(11) Orgel, L. *J. Chem. Soc.* **1959**, 3815.
(12) Lefebvre, I.; Lannoo, M.; Allan, G.; Ibanez, A.; Fourcade, J.; Jumas, J. C. *Phys. Rev. Lett.* **1987**, *59*, 2471.
(13) Lefebvre, I.; Szymanski, M. A.; Olivier-Fourcade, J.; Jumas, J. C. *Phys. Rev. B* **1998**, *58*, 1896.
(14) Watson, G. W.; Parker, S. C. *J. Phys. Chem. B* **1999**, *103*, 1258.
(15) Watson, G. W.; Parker, S. C.; Kresse, G. *Phys. Rev. B* **1999**, *59*, 8481.
(16) Seshadri, R.; Hill, N. A. *Chem. Mater.* **2001**, *13*, 2892.
(17) Waghmare, U. V.; Spaldin, N. A.; Kandpal, H. C.; Seshadri, R. *Phys. Rev. B* **2003**, *67*, 125111-1.
(18) Welk, M. E.; Norquist, A. J.; Arnold, F. P.; Stern, C. L.; Poeppelmeier, K. R. *Inorg. Chem.* **2002**, *41*, 5119.

10.1021/ic048428c CCC: $30.25
Published on Web 03/08/2005

Table 1. Crystallographic Data for $BaTi(IO_3)_6$, $LaTiO(IO_3)_5$, $Ba_2VO_2(IO_3)_4{\cdot}(IO_3)$, $K_2MoO_2(IO_3)_4$, and $BaMoO_2(IO_3)_4{\cdot}H_2O$

formula	$BaTi(IO_3)_6$	$LaTiO(IO_3)_5$	$Ba_2VO_2(IO_3)_4{\cdot}(IO_3)$	$K_2MoO_2(IO_3)_4$	$BaMoO_2(IO_3)_4{\cdot}H_2O$
fw	1234.64	1077.31	1232.12	905.74	980.88
space group	*R*-3 (No. 148)	$P2_1/n$ (No. 14)	$P2_1/c$ (No. 14)	$C2/c$ (No. 15)	$P2_1/n$ (No. 14)
a (Å)	11.4711(10)	7.4798(10)	7.5012(9)	12.959(2)	13.3368(17)
b (Å)	11.4711(10)	18.065(2)	33.032(4)	6.0793(9)	5.6846(7)
c (Å)	11.1465(17)	10.4843(14)	7.2150(9)	17.748(3)	18.405(2)
α (deg)	90	90	90	90	90
β (deg)	90	91.742(2)	116.612(2)	102.410(4)	103.636(2)
γ (deg)	120	90	90	90	90
V (Å^3)	1270.2(2)	1416.0(3)	1598.3(3)	1365.5(4)	1356.0(3)
Z	3	4	4	4	4
T (°C)	293.0(2)	293.0(2)	293.0(2)	293.0(2)	293.0(2)
λ (Å)	0.71073	0.71073	0.71073	0.71073	0.71073
ρ_{calcd} (g cm^{-3})	4.842	5.054	5.120	4.406	4.805
μ (mm^{-1})	13.811	14.528	15.192	10.684	12.996
$R(F)^a$	0.0221	0.0286	0.0369	0.0269	0.0274
$R_w(F_o^2)^b$	0.0580	0.0758	0.0848	0.0674	0.0616

^{a} $R(F) = \sum||F_o| - |F_c||/\sum|F_o|$. ^{b} $R_w(F_o^2) = [\sum w(F_o^2 - F_c^2)^2/\sum w(F_o^2)^2]^{1/2}$.

Table 2. Selected Bond Distances (Å) for $BaTi(IO_3)_6$, $LaTiO(IO_3)_5$, $Ba_2VO_2(IO_3)_4{\cdot}(IO_3)$, $K_2MoO_2(IO_3)_4$, and $BaMoO_2(IO_3)_4{\cdot}H_2O$

$BaTi(IO_3)_6$		$LaTiO(IO_3)_5$		$Ba_2VO_2(IO_3)_4{\cdot}(IO_3)$		$K_2MoO_2(IO_3)_4$		$BaMoO_2(IO_3)_4{\cdot}H_2O$	
I(1)−O(1)	1.791(5)	I(1)−O(1)	1.839(5)	I(1)−O(1)	1.816(7)	I(1)−O(1)	1.912(4)	I(1)−O(1)	1.813(4)
I(1)−O(2)	1.858(5)	I(1)−O(2)	1.831(5)	I(1)−O(2)	1.844(6)	I(1)−O(2)	1.828(4)	I(1)−O(2)	1.884(4)
I(1)−O(3)	1.808(5)	I(1)−O(4)	1.802(5)	I(1)−O(3)	1.808(7)	I(1)−O(2)	2.337(4)	I(1)−O(3)	1.786(4)
Ti(1)−O(2) × 6	1.939(5)	I(2)−O(5)	1.812(5)	I(2)−O(4)	1.832(7)	I(1)−O(3)	1.794(4)	I(2)−O(4)	1.897(4)
		I(2)−O(6)	1.826(5)	I(2)−O(5)	1.797(7)	I(2)−O(4)	1.840(4)	I(2)−O(5)	1.807(4)
		I(2)−O(7)	1.794(5)	I(2)−O(6)	1.809(7)	I(2)−O(5)	1.798(4)	I(2)−O(6)	1.779(4)
		I(3)−O(8)	1.819(5)	I(3)−O(7)	1.794(6)	I(2)−O(6)	1.784(4)	I(3)−O(7)	1.846(4)
		I(3)−O(9)	1.820(5)	I(3)−O(8)	1.866(6)	Mo(1)−O(1) × 2	1.955(4)	I(3)−O(8)	1.805(4)
		I(3)−O(10)	1.801(5)	I(3)−O(9)	1.802(7)	Mo(1)−O(4) × 2	2.238(4)	I(3)−O(9)	1.788(4)
		I(4)−O(3)	1.878(5)	I(4)−O(10)	1.816(7)	Mo(1)−O(7) × 2	1.710(4)	I(4)−O(10)	1.848(4)
		I(4)−O(11)	1.806(5)	I(4)−O(11)	1.802(7)			I(4)−O(11)	1.797(4)
		I(4)−O(12)	1.789(5)	I(4)−O(12)	1.788(7)			I(4)−O(12)	1.784(4)
		I(5)−O(14)	1.803(5)	I(5)−O(13)	1.822(6)			Mo(1)−O(2)	1.962(4)
		I(5)−O(15)	1.823(5)	I(5)−O(14)	1.796(7)			Mo(1)−O(4)	2.006(4)
		I(5)−O(16)	1.815(5)	I(5)−O(15)	1.784(7)			Mo(1)−O(7)	2.196(4)
		Ti(1)−O(1)	2.038(5)	V(1)−O(2)	1.975(6)			Mo(1)−O(10)	2.191(4)
		Ti(1)−O(3)	2.117(5)	V(1)−O(4)	2.245(7)			Mo(1)−O(13)	1.709(4)
		Ti(1)−O(6)	1.970(5)	V(1)−O(8)	1.975(6)			Mo(1)−O(14)	1.699(4)
		Ti(1)−O(9)	2.042(5)	V(1)−O(13)	2.164(7)				
		Ti(1)−O(13)	1.695(5)	V(1)−O(16)	1.639(7)				
		Ti(1)−O(15)	1.987(5)	V(1)−O(17)	1.646(7)				

observations regarding the out-of-center distortion of the d^0 transition metal.[19] First, the magnitude of the distortion scales as $Mo^{6+} > V^{5+} > W^{6+} > Nb^{5+} > Ta^{5+} > Ti^{4+}$, similar to the electronegativity of these cations.[20] Second, corner (C_4) and edge (C_2) type displacements are most commonly observed for Ti^{4+} and V^{5+}, whereas edge and face (C_3) distortions are preferred for Mo^{6+} and W^{6+}. All three types of distortions, edge, face, and corner, are found with Nb^{5+} and Ta^{5+}. Third, for the d^0 transition metal to undergo an out-of-center distortion, at least one of the oxide ligands needs to be terminal or bonded to another d^0 transition metal. In other words, when all six oxide ligands of the d^0 transition metal are further bonded to a lone pair cation, the transition metal is undistorted. We rationalized this by noting that the lone pair cation is in a "predistorted" coordination environment. Thus, any additional distortion would be unfavorable.

We report in this paper the synthesis, structure, and characterization of five new d^0 transition metal iodates, $BaTi(IO_3)_6$, $LaTiO(IO_3)_5$, $Ba_2VO_2(IO_3)_4{\cdot}(IO_3)$, $K_2MoO_2(IO_3)_4$, and $BaMoO_2(IO_3)_4{\cdot}H_2O$. We also examine the various cationic displacements and discuss these displacements with respect to primary and secondary distortion concepts.

Experimental Section

Reagents. K_2CO_3 (Alfa Aesar, 99%), $Ba(OH)_2{\cdot}8H_2O$ (Alfa Aesar, 98+%), La_2O_3 (99.9%), TiO_2 (Aldrich, 99.9+%), V_2O_5 (Aldrich, 98+%), MoO_3 (Aldrich, 99+%), and HIO_3 (Aldrich, 99.5+%) were used as received.

Syntheses. For $BaTi(IO_3)_6$, 0.500 g (1.58×10^{-3} mol) of $Ba(OH)_2{\cdot}8H_2O$, 0.200 g (2.50×10^{-3} mol) of TiO_2, and 5.000 g (2.84×10^{-2} mol) of HIO_3 were combined with 10 mL of H_2O. For $LaTiO(IO_3)_5$, 0.300 g (9.21×10^{-4} mol) of La_2O_3, 0.200 g (2.50×10^{-3} mol) of TiO_2, and 5.000 g (2.84×10^{-2} mol) of HIO_3 were combined with 10 mL of H_2O. For $Ba_2VO_2(IO_3)_4{\cdot}(IO_3)$, 0.500 g ($1.58 \times 10^{-3}$ mol) of $Ba(OH)_2{\cdot}8H_2O$, 0.200 g (1.10×10^{-3} mol) of V_2O_5, and 5.000 g (2.84×10^{-2} mol) of HIO_3 were combined with 10 mL of H_2O. For $K_2MoO_2(IO_3)_4$, 0.300 g (2.17×10^{-3} mol) of K_2CO_3, 0.300 g (2.08×10^{-3} mol) of MoO_3, and 5.000 g (2.84×10^{-2} mol) of HIO_3 were combined with 10 mL of H_2O. For $BaMoO_2(IO_3)_4{\cdot}H_2O$, 0.500 g ($1.58 \times 10^{-3}$ mol) of $Ba(OH)_2{\cdot}8H_2O$, 0.500 g (3.47×10^{-3} mol) of MoO_3, and 5.000 g (2.84×10^{-2} mol) of HIO_3 were combined with 10 mL of H_2O. The respective solutions were placed in 23-mL Teflon-lined autoclaves and subsequently sealed. The autoclaves were gradually heated to 230

(19) Halasyamani, P. S. *Chem. Mater.* **2004**, *16*, 3586.
(20) Eng, H. W.; Barnes, P. W.; Auer, B. M.; Woodward, P. M. *J. Solid State Chem.* **2003**, *175*, 94.

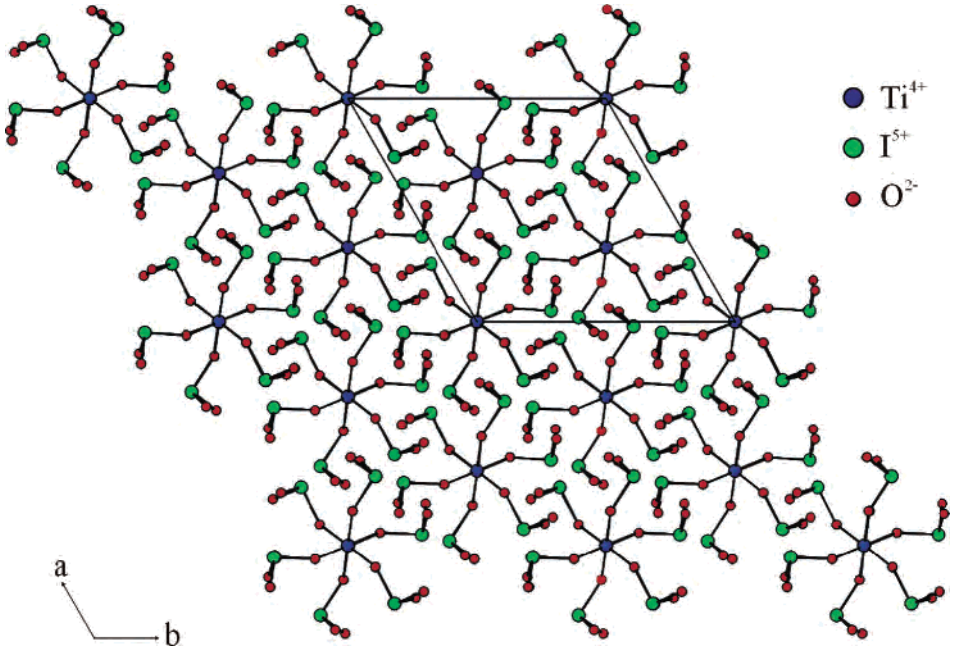

Figure 1. Ball-and-stick representation of $BaTi(IO_3)_6$ in the *ab*-plane. The Ba^{2+} cations have been removed for clarity.

°C, held for 4 d, and cooled slowly to room temperature at a rate of 6 °C h^{-1}. The mother liquor was decanted from the products. The products were recovered by filtration and washed with water and ethanol. For $Ba_2VO_2(IO_3)_4{\cdot}(IO_3)$, pale yellow plates crystals were found in 69% yield based on V_2O_5. For $BaTi(IO_3)_6$, $LaTiO(IO_3)_5$, $BaMoO_2(IO_3)_4{\cdot}H_2O$, and $K_2MoO_2(IO_3)_4$, colorless crystals, the only product from the reaction, were recovered in 79%, 81%, 78%, and 76% yields, respectively, based on the corresponding d^0 transition metal oxide.

Single-Crystal X-ray Diffraction. For $BaTi(IO_3)_6$ a colorless cube ($0.06 \times 0.08 \times 0.10$ mm^3), for $LaTiO(IO_3)_5$ a colorless block ($0.12 \times 0.16 \times 0.22$ mm^3), for $Ba_2VO_2(IO_3)_4{\cdot}(IO_3)$ a light yellow plate ($0.02 \times 0.06 \times 0.12$ mm^3), for $BaMoO_2(IO_3)_4{\cdot}H_2O$ a colorless block ($0.12 \times 0.20 \times 0.22$ mm^3), and for $K_2MoO_2(IO_3)_4$ a colorless block ($0.16 \times 0.22 \times 0.46$ mm^3) were used for single-crystal data analyses. Data were collected using a Siemens SMART diffractometer equipped with a 1K CCD area detector using graphite monochromated Mo Kα radiation. A hemisphere of data was collected using a narrow-frame method with scan widths of 0.30° in ω, and an exposure time of 25 s per frame. The first 50 frames were remeasured at the end of the data collection to monitor instrument and crystal stability. The maximum correction applied to the intensities was <1%. The data were integrated using the Siemens SAINT program,[21] with the intensities corrected for Lorentz, polarization, air absorption, and absorption attributable to the variation in the path length through the detector faceplate. ψ-scans were used for the absorption correction on the hemisphere of data. The data were solved and refined using SHELXS-97 and SHELXL-97, respectively.[22,23] All of the atoms were refined with anisotropic thermal parameters and converged for $I > 2\sigma(I)$. All calculations were performed using the WinGX-98 crystallographic software package.[24] During the course of the refinement for $BaTi(IO_3)_6$, we determined that fractional occupancy must occur in the barium atoms to retain charge balance. Fractional occupancy of 0.500(3) was refined for Ba^{2+}. Relevant crystallographic data and selected bond distances are given in Tables 1 and 2, respectively.

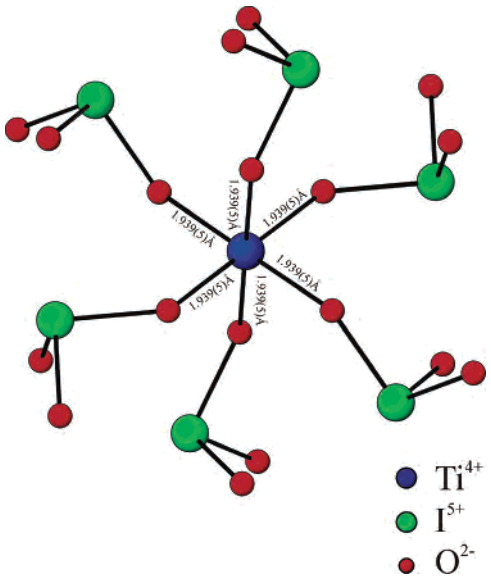

Figure 2. Ball-and-stick representation of the $[Ti(IO_3)_6]^{2-}$ anionic unit in $BaTi(IO_3)_6$. All six oxide ligands linked to Ti^{4+} are also bonded to an I^{5+} cation. Thus, the Ti^{4+} cation is in an undistorted environment with six equal Ti−O bonds.

Powder X-ray Diffraction. Powder X-ray diffraction was used to confirm the phase purity of each sample. The X-ray powder diffraction data were collected on a Scintag XDS2000 diffractometer at room temperature (Cu Kα radiation, $\theta-\theta$ mode, flat plate geometry) equipped with Peltier germanium solid-state detector in the 2θ range 5−60° with a step size of 0.02°, and a step time of 1 s.

Infrared and Raman Spectroscopy. Infrared spectra were recorded on a Matteson FTIR 5000 spectrometer in the 400−4000 cm^{-1} range, with the sample pressed between two KBr pellets. Raman spectra were recorded at room temperature on a Digilab

(21) *SAINT*, *version 4.05*: *Program for Area Detector Absorption Correction*; Siemens Analytical X-ray Instruments: Madison, WI, 1995.
(22) Sheldrick, G. M. *SHELXS-97-A program for automatic solution of crystal structures*; University of Goettingen: Goettingen, Germany, 1997.
(23) Sheldrick, G. M. *SHELXL-97-A program for crystal structure refinement*; University of Goettingen: Goettingen, Germany, 1997.
(24) Farrugia, L. J. *J. Appl. Crystallogr.* **1999**, *32*, 837.

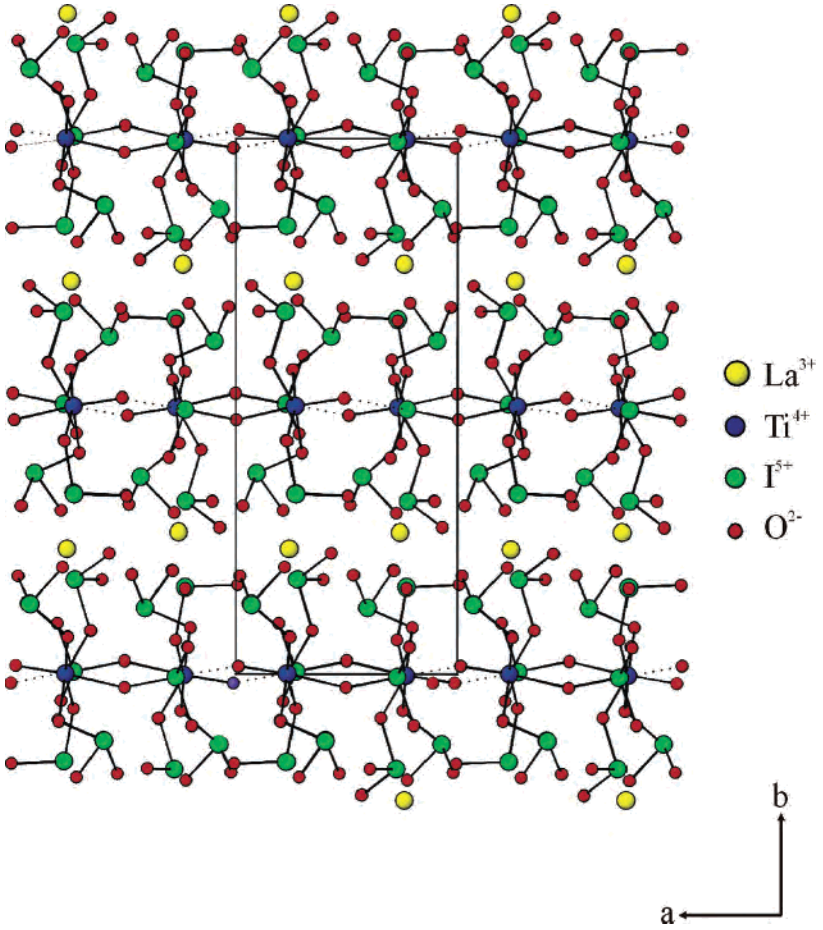

Figure 3. Ball-and-stick representation of $LaTiO(IO_3)_5$ in the *ab*-plane. The dashed lines indicate long I−O interactions giving the structure a pseudo-one-dimensional topology.

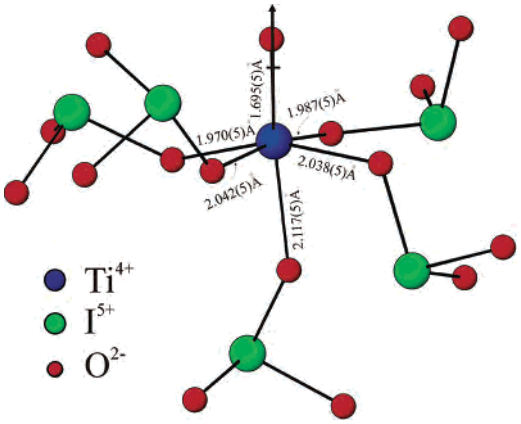

Figure 4. Ball-and-stick representation of the $[TiO(IO_3)_5]^{3-}$ anionic unit in $LaTiO(IO_3)_5$. Note that the Ti^{4+} undergoes an out-of-center displacement toward an apical oxide ligand, along the local C_4 direction. The arrow indicates the approximate direction of the local dipole moment in the TiO_6 octahedron.

FTS 7000 spectrometer equipped with a germanium detector with the powder sample placed in separate capillary tubes. Excitation was provided by a Nd:YAG laser at a wavelength of 1064 nm, and the output laser power was 500 mW. The spectral resolution was ~4 cm^{-1}, and 100 scans were collected for each sample.

UV−Vis Diffuse Reflectance Spectroscopy. UV−vis diffuse reflectance data for all of the reported crystalline samples were collected with a Varian Cary 500 scan UV−vis−NIR spectrophotometer over the spectral range 200−1500 nm at room temperature. Poly(tetrafluoroethylene) was used as a reference material. Reflectance spectra were converted to absorbance with the Kubelka−Munk values.[25]

Thermogravimetric Analysis. Thermogravimetric analyses were carried out on a TGA 2950 thermogravimetric analyzer (TA instruments). The sample was contained within a platinum crucible and heated in air at a rate of 10 °C min^{-1} to 800 °C.

Results

Structures. $BaTi(IO_3)_6$. The zero-dimensional $BaTi(IO_3)_6$ consists of a TiO_6 octahedron linked to six IO_3 polyhedra that are separated by Ba^{2+} cations (see Figure 1). In connectivity terms, the structure may be written as $\{[TiO_{6/2}]^{2-}6[IO_{1/2}O_{2/1}]^0\}^{2-}$, with charge balance maintained by the Ba^{2+} cations. Each Ti^{4+} cation is bonded to six oxygen atoms in an octahedral environment with a unique Ti−O bond distance of 1.939(5) Å. All six oxygen atoms linked to the Ti^{4+} cation are further bonded to an I^{5+} cation. The I^{5+} cations are bonded to three oxygen atoms in a distorted trigonal pyramidal environment with I−O bond distances ranging from 1.791(5) to 1.858(5) Å (see Figure 2). The bond distances are consistent with similar compounds previously reported.[26−31] Bond valence calculations[32,33] resulted in values of 2.22, 4.95, and 4.29 for Ba^{2+}, I^{5+}, and Ti^{4+}, respectively.

(25) Kubelka, P.; Munk, F. *Z. Tech. Phys.* **1931**, *12*, 593.
(26) Schellhaas, F.; Hartl, H.; Frydrych, R. *Acta Crystallogr.* **1972**, *B28*, 2834.
(27) Alcock, N. W. *Acta Crystallogr.* **1972**, *B28*, 2783.

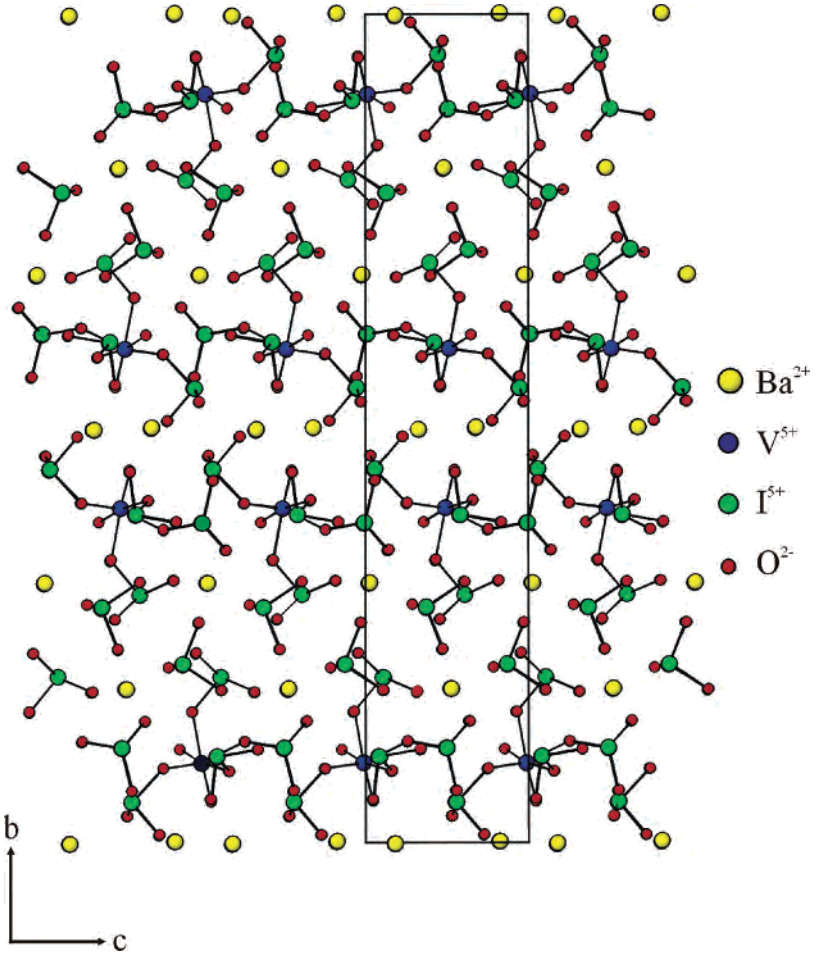

Figure 5. Ball-and-stick representation of $Ba_2VO_2(IO_3)_4 \cdot (IO_3)$ in the *bc*-plane. Note the "free" $[IO_3]^-$ anionic groups between the molecular units.

$LaTiO(IO_3)_5$. This d^0 transition metal iodate exhibits a pseudo-one-dimensional structure consisting of a TiO_6 octahedron linked to five IO_3 polyhedra that are separated by La^{3+} cations (see Figure 3). In connectivity terms, the structure may be written as $\{[TiO_{5/2}O_{1/1}]^{3-}\ 5[IO_{1/2}O_{2/1}]^0\}^{3-}$, with charge balance maintained by the La^{3+} cation. Each Ti^{4+} is bonded to six oxygen atoms in an octahedral environment with one "short" (1.695(5) Å), four "normal" (1.970(5)−2.042(5) Å), and one "long" bond (2.117(5) Å). Five of the six oxygen atoms are further bonded to an I^{5+} cation, whereas the sixth, the "short" Ti−O bond, remains "terminal". The Ti^{4+} cation displaces toward the terminal oxygen atom, thereby undergoing an out-of-center distortion toward a corner of its oxide octahedron, that is, a C_4 distortion (see Figure 4). We will be discussing all of the various cationic distortions later in the paper. The I^{5+} cations are linked to three oxygen atoms in a distorted trigonal pyramidal environment with I−O bond distances ranging from 1.794(5) to 1.878(5) Å (see Figure 4). There is one long I−O contact of 2.197(5) Å that has been drawn as a dashed line in Figure 3. This long contact effectively links the TiO_6 octahedra, through this "IO_4" group, and gives $LaTiO(IO_3)_5$ a pseudo-one-dimensional topology. Bond valence calculations[32,33] resulted in values of 3.14 for La^{3+}, 5.01−5.48 for I^{5+}, and 4.20 for Ti^{4+}.

$Ba_2VO_2(IO_3)_4 \cdot (IO_3)$. Similar to $BaTi(IO_3)_6$, $Ba_2VO_2(IO_3)_4 \cdot (IO_3)$ also exhibits a zero-dimensional structure that consists of a VO_6 octahedron linked to four IO_3 groups (see Figure 5). In connectivity terms, the structure maybe written as $\{[VO_{2/1}O_{4/2}]^{3-}\ 4[IO_{2/1}O_{1/2}]^0 \cdot [IO_{3/1}]^-\}^{4-}$, with charge balance retained by two Ba^{2+} cations. Unlike the other zero-dimensional compounds reported in this paper, $Ba_2VO_2(IO_3)_4 \cdot (IO_3)$ has a completely unbound IO_3^- anion, that is, $[IO_{3/1}]^-$, that interacts with the Ba^{2+} cations. Each V^{5+} is bonded to six oxygen atoms in an octahedral environment, with two "short" V−O bonds of 1.639(7) and 1.646(7) Å, two "normal" bonds of 1.975(6) Å × 2, and two "long" bonds of 2.164(7) and 2.245(7) Å (see Figure 6). Four of the six oxygen atoms are further bonded to an I^{5+} cation, whereas the remaining two, the "short" V−O bonds, are terminal. The V^{5+} undergoes an out-of-center distortion, in the direction of the terminal oxygen atoms, toward an edge of its octahedron, that is, a C_2 distortion (see Figure 6). The I^{5+} cations are linked to three oxygen atoms in a distorted trigonal pyramidal environment with I−O bond distances ranging from 1.784(7) to 1.866(6) Å. Bond valence calcula-

(28) Coquet, E.; Crettez, J. M.; Pannetier, J.; Bouillot, J.; Damien, J. C. *Acta Crystallogr.* **1983**, *B39*, 408.
(29) Lucas, B. W. *Acta Crystallogr.* **1984**, *C40*, 1989.
(30) Svensson, C.; Stahl, K. *J. Solid State Chem.* **1988**, *77*, 112.
(31) Stahl, K.; Szafranski, M. *Acta Chem. Scand.* **1992**, *46*, 1146.
(32) Brown, I. D.; Altermatt, D. *Acta Crystallogr.* **1985**, *B41*, 244.
(33) Brese, N. E.; O'Keeffe, M. *Acta Crystallogr.* **1991**, *B47*, 192.

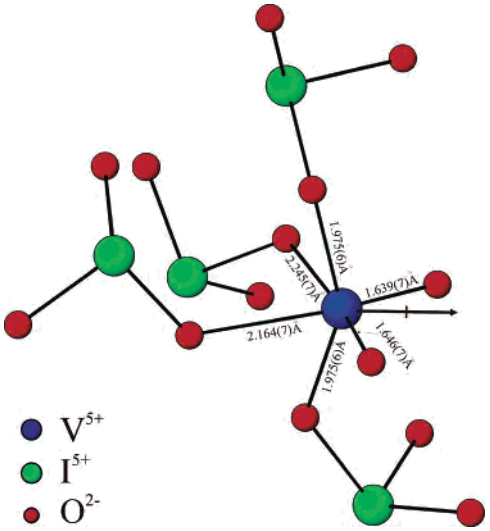

Figure 6. Ball-and-stick representation of the $[VO_2(IO_3)_4]^{3-}$ anionic unit in $Ba_2VO_2(IO_3)_4 \cdot (IO_3)$. Note that the V^{5+} undergoes an out-of-center displacement toward two equatorial oxide ligands, along the local C_2 direction. The arrow indicates the direction of the local dipole moment in the VO_6 octahedron.

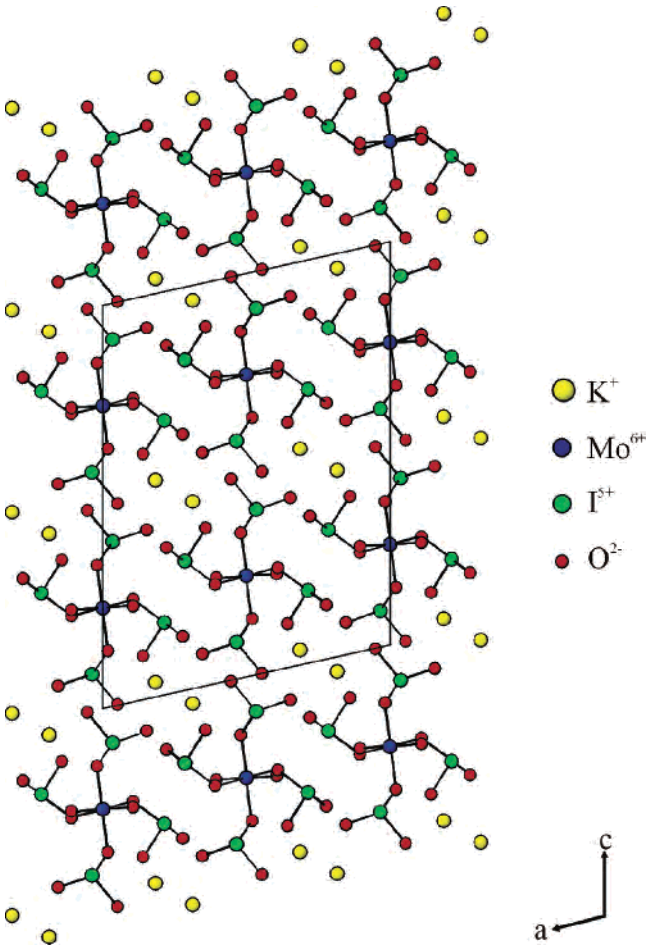

Figure 7. Ball-and-stick representation of $K_2MoO_2(IO_3)_4$ in the *ac*-plane. The K^+ cations separate the $[MoO_2(IO_3)_4]^{2-}$ anionic units.

tions[32,33] resulted in values of 2.07 and 2.08 for Ba^{2+}, 4.89−5.19 for I^{5+}, and 5.02 for V^{5+}.

$K_2MoO_2(IO_3)_4$. A zero-dimensional structure is also exhibited by $K_2MoO_2(IO_3)_4$, where a MoO_6 octahedron is linked to four IO_3 polyhedra (see Figure 7), that are separated

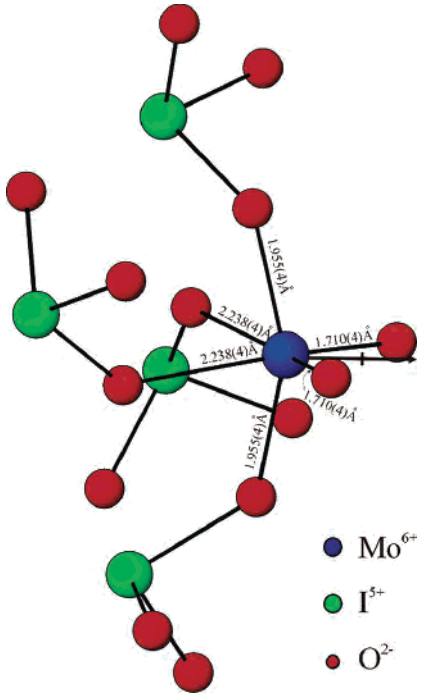

Figure 8. Ball-and-stick representation of the $[MoO_2(IO_3)_4]^{2-}$ anionic unit in $K_2MoO_2(IO_3)_4$. Note that the Mo^{6+} undergoes an out-of-center displacement toward two equatorial oxide ligands, along the local C_2 direction. The arrow indicates the direction of the local dipole moment in the MoO_6 octahedron.

by K^+ cations. In connectivity terms, the structure may be written as $\{[MoO_{2/1}O_{4/2}]^{2-}\ 4[IO_{2/1}O_{1/2}]^0\}^{2-}$, with charge balance retained by two K^+ cations. Each Mo^{6+} cation is bonded to six oxygen atoms in an octahedral environment with two "short" Mo−O bonds of 1.710(4) Å × 2, two "normal" bonds of 1.955(4) Å × 2, and two "long" bonds of 2.238(4) Å × 2. Similar to the V^{5+} cations in $Ba_2VO_2(IO_3)_4 \cdot (IO_3)$, four of the six oxygen atoms are further bonded to an I^{5+} cation, whereas the remaining two oxygen atoms are terminal. The Mo^{6+} undergoes an out-of-center distortion, in the direction of the terminal oxygen atoms, toward the edge of its octahedron, that is, a C_2 distortion (see Figure 8). The I^{5+} cations are linked to three oxygen atoms in a distorted trigonal pyramidal environment with I−O bond distances ranging from 1.784(4) to 1.912(4) Å. Bond valence calculations[32,33] resulted in values of 1.18 for K^+, 5.05 and 5.10 for I^{5+}, and 5.98 for Mo^{6+}.

$BaMoO_2(IO_3)_4 \cdot H_2O$. This mixed-metal iodate is topologically very similar to $K_2MoO_2(IO_3)_4$. $BaMoO_2(IO_3)_4 \cdot H_2O$ exhibits a zero-dimensional structure consisting of a MoO_6 octahedron linked to four IO_3 groups that are separated by H_2O molecules and Ba^{2+} cations (see Figure 9). In connectivity terms, the structure may be written as $\{[MoO_{4/2}O_{2/1}]^{2-}\ 4[IO_{2/1}O_{1/2}]^0\}^{2-}$, with charge balance retained by the Ba^{2+} cation. Each Mo^{6+} cation is bonded to six oxygen atoms in an octahedral environment with two "short" Mo−O bonds of 1.699(4) and 1.709(4) Å, two "normal" bonds of 1.962(4) and 2.006(4) Å, and two "long" bonds of 2.191(4) and 2.196(4) Å. The short Mo−O bonds are terminal, whereas the remaining four link to the IO_3 polyhedra. Again, the Mo^{6+} cation displaces in the direction of the terminal oxygen atoms,

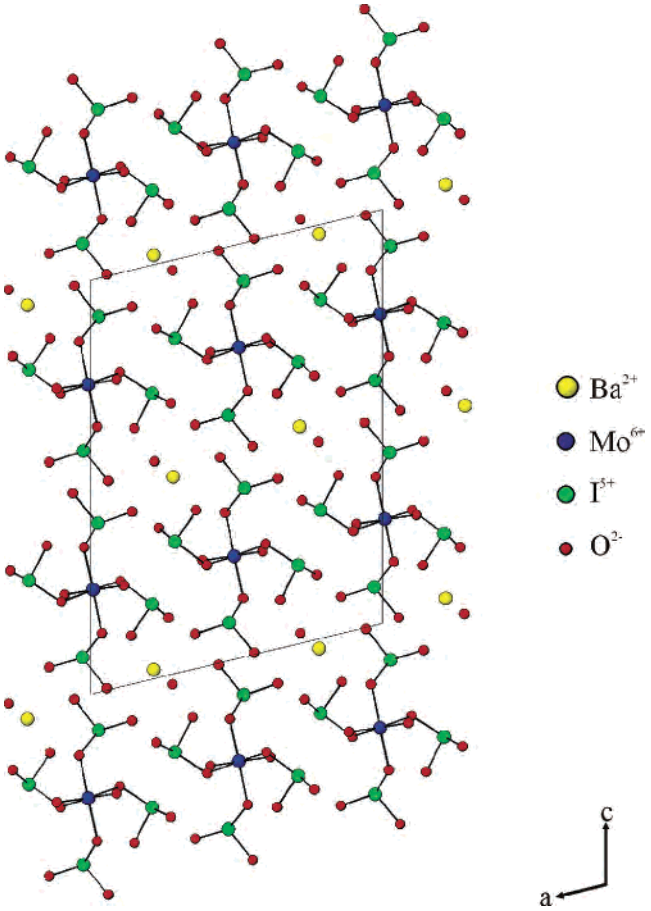

Figure 9. Ball-and-stick representation of $BaMoO_2(IO_3)_4 \cdot H_2O$ in the *ac*-plane. The Ba^{2+} cations and H_2O molecules separate the $[MoO_2(IO_3)_4]^{2-}$ anionic units.

toward the edge of its octahedron, that is, a C_2 distortion (see Figure 10). The I^{5+} cations are linked to three oxygen atoms in a distorted trigonal pyramidal environment with I−O bond distances ranging from 1.779(4) to 1.897(4) Å. Bond valence calculations[32,33] resulted in values of 1.78 for Ba^{2+}, 4.85−5.07 for I^{5+}, and 6.01 for Mo^{6+}.

Infrared and Raman Spectroscopy. The infrared and Raman spectra of $BaTi(IO_3)_6$, $LaTiO(IO_3)_5$, $Ba_2VO_2(IO_3)_4 \cdot (IO_3)$, $K_2MoO_2(IO_3)_4$, and $BaMoO_2(IO_3)_4 \cdot H_2O$ reveal Ti−O, V−O, and Mo−O vibrations in the regions ca. 700, 700−900, and 700−940 cm^{-1}, respectively. The stretches 620−830 and 360−560 cm^{-1} can be attributed to I−O vibrations. The infrared and Raman vibrations and assignments are listed in Table 3. The assignments are consistent with those previously reported.[34−40]

(34) Sykora, R. E.; Ok, K. M.; Halasyamani, P. S.; Wells, D. M.; Albrecht-Schmitt, T. E. *Chem. Mater.* **2002**, *14*, 2741.
(35) Sykora, R. E.; Ok, K. M.; Halasyamani, P. S.; Albrecht-Schmitt, T. E. *J. Am. Chem. Soc.* **2002**, *124*, 1951.
(36) Shehee, T. C.; Sykora, R. E.; Ok, K. M.; Halasyamani, P. S.; Albrecht-Schmitt, T. E. *Inorg. Chem.* **2003**, *42*, 457.
(37) Maggard, P. A.; Kopf, A. L.; Stern, C. L.; Poeppelmeier, K. R.; Ok, K. M.; Halasyamani, P. S. *Inorg. Chem.* **2002**, *41*, 4852.
(38) Guarany, C. A.; Pelaio, L. H. Z.; Araujo, E. B.; Yukimitu, K.; Moraes, J. C. S.; Eiras, J. A. *J. Phys.: Condens. Matter* **2003**, *15*, 4851.
(39) Rasmussen, S. B.; Rasmussen, R. M.; Fehrmann, R.; Nielsen, K. *Inorg. Chem.* **2003**, *42*, 7123.
(40) Rasmussen, S. B.; Boghosian, S.; Nielsen, K.; Eriksen, K. M.; Fehrmann, R. *Inorg. Chem.* **2004**, *43*, 3697.

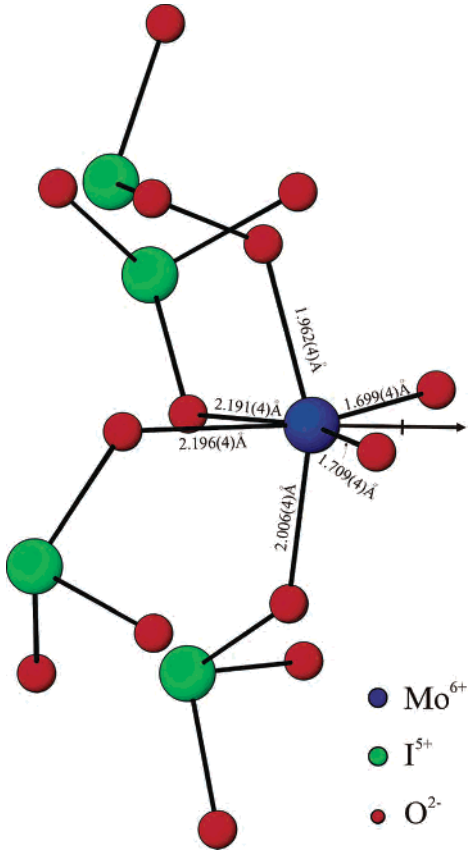

Figure 10. Ball-and-stick representation of the $[MoO_2(IO_3)_4]^{2-}$ anionic unit in $BaMoO_2(IO_3)_4 \cdot H_2O$. Note that the Mo^{6+} undergoes an out-of-center displacement toward two equatorial oxide ligands, along the local C_2 direction. The arrow indicates the direction of the local dipole moment in the MoO_6 octahedron.

UV−Vis Diffuse Reflectance Spectroscopy. The UV−vis diffuse reflectance spectra for all of the reported iodates have been deposited in the Supporting Information. All of the compounds are white with the exception of $Ba_2VO_2(IO_3)_4 \cdot (IO_3)$, which is light yellow. These spectra show that the iodate compounds are transparent to approximately 3.2−3.8 eV. Absorption (*K*/*S*) data were calculated from the following Kubelka−Munk function:

$$F(R) = \frac{(1-R)^2}{2R} = \frac{K}{S}$$

with *R* representing the reflectance, *K* the absorption, and *S* the scattering. In a *K*/*S* versus *E* (eV) plot, extrapolating the linear part of the rising curve to zero provides the onset of absorption at 3.3, 3.4, 3.2, 3.6, and 3.8 eV for $BaTi(IO_3)_6$, $LaTiO(IO_3)_5$, $Ba_2VO_2(IO_3)_4 \cdot (IO_3)$, $BaMoO_2(IO_3)_4 \cdot H_2O$, and $K_2MoO_2(IO_3)_4$, respectively. The overall band gap for each material may be attributable to the degree of Ti (3d), V (3d), and Mo (4d) orbitals as well as the distortions of crystal structures arising from IO_3 polyhedra. $LaTiO(IO_3)_5$, however, reveals a small shoulder near the main absorption band, suggesting an indirect transition.

Thermogravimetric Analysis. All of the iodate compounds reported in this paper are not stable at higher temperatures. With each material, decompositions through thermal disproportionation occurred between 400 and 460

Table 3. Infrared and Raman Vibrations (cm^{-1}) for $BaTi(IO_3)_6$, $LaTiO(IO_3)_5$, $Ba_2VO_2(IO_3)_4{\cdot}(IO_3)$, $K_2MoO_2(IO_3)_4$, and $BaMoO_2(IO_3)_4{\cdot}H_2O$

$BaTi(IO_3)_6$		$LaTiO(IO_3)_5$		$Ba_2VO_2(IO_3)_4{\cdot}(IO_3)$		$K_2MoO_2(IO_3)_4$		$BaMoO_2(IO_3)_4{\cdot}H_2O$		
Ti−O	I−O	Ti−O	I−O	V−O	I−O	Mo−O	I−O	Mo−O	I−O	O−H
					IR (cm^{-1})					
698	821	700	836	1166	827	925	819	937	827	3563
588	813	568	819	901	815	885	769	914	815	3502
503	779	493	808	881	771	715	744	892	777	1604
	769		794	869	761	638	431	561	763	
	649		771	794	742	511	412	499	740	
	457		748	709	455	495			713	
	439		642	682	433				644	
	424		451	489	418				474	
	416		424						420	
					Raman (cm^{-1})					
717	821	713	813	898	821	921	825	933	821	
671	806	690	806	879	775	875	806	910	802	
513	779		759	790	744	705	763	883	779	
	752		740	713	447		748	725	763	
	640		624	675	428		663	698	740	
	408		482	486	416		505		655	
	366		462				420		505	
			412				401		482	
			389				389		424	
									412	

°C. For $BaTi(IO_3)_6$, 2 equiv of I_2 and 5 equiv of O_2 are lost at approximately 420 °C: calc.(exp.) 54.07%(54.26%). The remainder of the I_2 and O_2 are lost at approximately 530 °C: calc.(exp.) 58.87%(58.53%). For $BaTi(IO_3)_6$, $BaTiO_3$ remains above 800 °C. With $LaTiO(IO_3)_5$, 2 equiv of O_2 is lost at approximately 400 °C, calc.(exp.) 5.94%(5.75%). Next, 1 equiv of I_2 and another 1.5 equiv of O_2 are lost at around 570 °C, calc.(exp.) 29.78% (29.68%). Finally, the remainder of I_2 and O_2 are lost, leaving a mixture of La_2O_3 and TiO_2 at around 800 °C: calc.(exp.) 65.88%(66.02%). $Ba_2VO_2(IO_3)_4{\cdot}(IO_3)$ loses 1 mol of I_2 and 2.75 mol of O_2 at around 460 °C: calc.(exp.) 27.74%(28.13%). Next, 0.5 mol of I_2 and 1.75 mol of O_2 are subsequently lost at approximately 540 °C: calc.(exp.) 20.54%(20.24%). The remainder of I_2 and O_2 are lost at around 800 °C, leaving a mixture of BaO and V_2O_5: calc.(exp.) 43.79%(43.84%). With $K_2MoO_2(IO_3)_4$, single step decomposition occurs at around 400 °C, indicating the loss of 2 mol of I_2 and 5 mol of O_2: calc.(exp.) 73.71%(73.64%). $BaMoO_2(IO_3)_4{\cdot}H_2O$ shows a weight loss at 330 °C that is attributed to the loss of the occluded water molecules from the materials: calc.-(exp.) 1.83%(1.93%). Next, 2 equiv of I_2 and 5 equiv of O_2 are lost at approximately 410 °C, leaving a mixture of BaO and MoO_3 at 800 °C: calc.(exp.) 69.19%(69.89%). The TGA curves for all five materials have been deposited in the Supporting Information.

Discussion

In all of the reported materials, the d^0 transition metal is in an octahedral coordination environment bonded to six oxygen atoms. The oxide ligands are either terminal or bonded to an I^{5+} cation. As previously discussed, primary and secondary distortion concepts can be used to better understand these materials. For the reported materials, the primary distortion is the electronic (SOJT) distortion that occurs for both the d^0 transition metal and the I^{5+} cation, whereas the secondary distortion is the interaction between the oxide octahedra and the IO_3 polyhedra. In oxide materials that contain d^0 transition metals and lone pair cations, the direction and magnitude of the out-of-center displacement of the d^0 transition metal depend on the coordination of the oxide ligands as well as the particular d^0 transition metal.[19] In materials where all six oxide ligands are further bonded to a lone pair cation, we noted that the d^0 transition metal is undistorted, effectively "trapped" in the center of its coordination polyhedra. In other words, the secondary distortion overrides the primary distortion of the d^0 transition metal. This is precisely the situation that occurs in $BaTi(IO_3)_6$ (see Figure 2). In $BaTi(IO_3)_6$, all six oxide ligands surrounding Ti^{4+} are further bonded to an I^{5+} cation. If the Ti^{4+} cation were to distort toward one or more of the oxide ligands, a compensating distortion within an IO_3 group would be required. Because the IO_3 polyhedra are already "predistorted", attributable to the lone pair, any additional distortion would be unfavorable. Thus, the Ti^{4+} in $BaTi(IO_3)_5$ remains in the center of its oxide octahedron with six equal Ti−O bonds of 1.939(5) Å (see Figure 2).

Table 4. Direction and Magnitude of the d^0 Transition Metal Intra-Octahedral Distortion in $BaTi(IO_3)_6$, $LaTiO(IO_3)_5$, $Ba_2VO_2(IO_3)_4{\cdot}(IO_3)$, $K_2MoO_2(IO_3)_4$, and $BaMoO_2(IO_3)_4{\cdot}H_2O$

compound	direction − cation	magnitude
$BaTi(IO_3)_6$	no distortion − Ti^{4+}	0.00
$LaTiO(IO_3)_5$	C_4 − Ti^{4+}	0.55
$Ba_2VO_2(IO_3)_4{\cdot}(IO_3)$	C_2 − V^{5+}	1.16
$K_2MoO_2(IO_3)_4$	C_2 − Mo^{6+}	1.09
$BaMoO_2(IO_3)_4{\cdot}H_2O$	C_2 − Mo^{6+}	1.06

With the other materials, $LaTiO(IO_3)_5$, $BaVO_2(IO_3)_4{\cdot}(IO_3)$, $K_2MoO_2(IO_3)_4$, and $BaMoO_2(IO_3){\cdot}H_2O$, the d^0 transition metal, Ti^{4+}, V^{5+}, or Mo^{6+}, respectively, is displaced from the center of its oxide octahedron. The direction and magnitude of these distortions are consistent with those observed earlier for this class of compounds (see Table 4).[19] With Ti^{4+}, in $LaTiO(IO_3)_5$, the cation is displaced toward an apical, terminal, oxygen atom, along the local C_4 direction (see Figure 4). This C_4−Ti^{4+} type displacement is the most

common for Ti^{4+}. The magnitude of this C_4-Ti^{4+} distortion is 0.55 (using the methodology outlined earlier),[19] which is larger than the average distortion observed for Ti^{4+}. Very similar types of distortions are observed in $BaVO_2(IO_3)_4 \cdot (IO_3)$, $K_2MoO_2(IO_3)_4$, and $BaMoO_2(IO_3) \cdot H_2O$ for V^{5+} and Mo^{6+}, respectively. In all three materials, the distortions are toward the two terminal oxide ligands, along the local C_2 direction (see Figures 6, 8, and 10). These C_2-V^{5+} and C_2-Mo^{6+} distortions are commonly observed for both cations. The magnitudes of the distortions are very large, >1.0, consistent with our previous observations.[19]

Acknowledgment. We thank the Robert A. Welch Foundation for support. This work was also supported by the NSF-Career Program through DMR-0092054. P.S.H. is a Beckman Young Investigator. We also acknowledge Jason Locklin and Prof. Rigoberto Advincula for assistance in obtaining the Raman spectra.

Note Added after ASAP: After this paper had been published on the Web (March 8, 2005), it was brought to our attention that the synthesis and structure of $K_2MoO_2(IO_3)_4$ was previously published by Sykora et al. (*J. Solid State Chem.* **2002**, *166*, 442). In addition, $BaTi(IO_3)_6$ is structurally similar to compounds reported by Schellhaas et al. (*Acta Crystallogr.* **1972**, *B28*, 2834) and Shehee et al. (*J. Alloys Compd.* **2005**, *388*, 225). We regret the omissions. The Web version published on March 23, 2005, and the print version of the article are correct.

Supporting Information Available: X-ray crystallographic files for $BaTi(IO_3)_6$, $LaTiO(IO_3)_5$, $Ba_2VO_2(IO_3)_4 \cdot (IO_3)$, $K_2MoO_2(IO_3)_4$, and $BaMoO_2(IO_3)_4 \cdot H_2O$ in CIF format, ORTEP diagrams, calculated and observed X-ray diffraction patterns, thermogravimetric analysis diagrams, UV−vis spectra, a bond valence table, and IR spectra for all of the compounds. This material is available free of charge via the Internet at http://pubs.acs.org.

IC048428C